metals

MDPI

Article

Temperature-Dependent Mechanical Properties of CoCrFeNi Medium-Entropy Alloy Produced by Laser-Directed Energy Deposition

Margarita Klimova [1,2,*], Igor Krasanov [1], Ilya Astakhov [1,2], Ekaterina Kovalenko [1], Elizaveta Kochura [1], Anastasia Semenyuk [1,2], Sergey Zherebtsov [1,2], Olga Klimova-Korsmik [1] and Nikita Stepanov [1,2]

[1] World-Class Research Center, "Advanced Digital Technologies", Saint Petersburg State Marine Technical University, 190121 Saint Petersburg, Russia; krasanov@ilwt.smtu.ru (I.K.); astakhov@bsu.edu.ru (I.A.); kovalenko.ek@inbox.ru (E.K.); kochura@ilwt.smtu.ru (E.K.); semenyuk@bsu.edu.ru (A.S.); zherebtsov@bsu.edu.ru (S.Z.); o.klimova@corp.smtu.ru (O.K.-K.); stepanov@bsu.edu.ru (N.S.)

[2] Laboratory of Bulk Nanostructured Materials, Belgorod State University, 308015 Belgorod, Russia

* Correspondence: klimova_mv@bsu.edu.ru

Abstract: The temperature dependence of the mechanical properties of the CoCrFeNi medium-entropy alloy (MEA) manufactured by laser-directed energy deposition (L-DED) and additionally annealed at 1200 °C for 24 h was studied. The microstructure of the as-deposited alloy was represented by a single-phase face-centered cubic structure with coarse columnar grains and a high density of dislocation. Annealing resulted in the development of recrystallization and a reduction in dislocation density. The CoCrFeNi alloy produced by L-DED demonstrated mechanical properties comparable with those of the fine-grained equiatomic CoCrFeMnNi alloy, produced by casting followed by thermomechanical processing. Namely, as-deposited CoCrFeNi had a yield strength (YS) and ultimate tensile strength (UTS) of YS = 370 MPa and UTS = 610 MPa at room temperature, and YS = 565 MPa and UTS = 965 MPa at cryogenic temperature, along with a ductility of ~60%. Annealing resulted in a decrease in strength to YS = 180/350 MPa at 293/77 K. A quantitative analysis of various strengthening mechanisms showed that some strength increment of the as-deposited alloy was ensured by the high dislocation density formed during L-DED.

Keywords: high-entropy alloys; medium-entropy alloys; laser-directed energy deposition; mechanical properties

Academic Editor: Jiro Kitagawa

Received: 22 November 2024
Revised: 18 December 2024
Accepted: 25 December 2024
Published: 27 December 2024

Citation: Klimova, M.; Krasanov, I.; Astakhov, I.; Kovalenko, E.; Kochura, E.; Semenyuk, A.; Zherebtsov, S.; Klimova-Korsmik, O.; Stepanov, N. Temperature-Dependent Mechanical Properties of CoCrFeNi Medium-Entropy Alloy Produced by Laser-Directed Energy Deposition. *Metals* **2025**, *15*, 9. https://doi.org/10.3390/met15010009

1. Introduction

A new class of materials, so-called multicomponent alloys, which first was introduced 20 years ago [1,2], still attracts great attention from material scientists around the world. It was first believed that high configuration entropy, achieved by multicomponent alloying, should suppress the formation of intermetallic phases, thereby promoting the formation of substitutional solid solutions. Alloys, consisting of five or more components in equimolar or near-equimolar ratios, are called high-entropy alloys (HEAs), whereas alloys with four or fewer are called medium-entropy alloys (MEAs). Despite that the influence of configurational entropy on the phase stability of multicomponent equiatomic alloys is not decisive [3], the M/HEAs designation is still widely used, especially for alloys with single solid solution structures [4].

Based on 3D transition elements, alloys are probably the most studied system among the HEAs/MEAs classes [3–5]. One of the typical examples is the equiatomic CoCrFeMnNi

Cantor alloy with a single (stable at T $\geq$ 900 °C with possible precipitation of secondary phases below [6,7]) face-centered cubic (fcc) phase structure which has a very high ductility and fracture toughness at room and cryogenic temperatures [2,8]. The influence of various equiatomic elemental combinations on the phase stability, microstructural evolution, and mechanical properties of the Co-Cr-Fe-Mn-Ni system alloys have been extensively studied [3,9,10]. It was shown that the properties do not have a direct dependence on the number of elements (i.e., value of configuration entropy) but are determined to a greater extent by the choice of the constitutive elements, which in turn strongly affect the lattice friction and the operating deformation mechanisms [11,12]. For example, increasing the number of elements in an alloy from four (CoCrFeNi or CoCrNiMn) to five (CoCrFeMnNi) changed the mechanical behavior slightly, while the most attractive properties were found in the three-component alloy (NiCoCr) [9,13,14].

In general, CoCrFeMnNi-based alloys with the single fcc phase structure have a rather low yield strength at room temperature, which significantly increases in cryogenic conditions without a noticeable drop in ductility [8,15]. As is known, improving mechanical properties at cryogenic temperatures was associated with the activation of the twinning-induced plasticity (TWIP) effect due to the low stacking-fault energy (SFE) of these alloys [16–19]. Development of deformation twinning resulted in the excellent strain-hardening capacity of HEAs, making these materials promising for cryogenic applications [12,20,21]. Therefore, one of the main ways to improve the strength of single-phase HEAs/MEAs, produced by conventional processing techniques, is some microstructure refinement via thermomechanical processing [16,22]. The formation of a partially recrystallized structure due to cold rolling followed by annealing provides an outstanding combination of high strength and ductility of CoCrFeMnNi-based alloys [23,24]. However, the required large deformation strains increase the labor intensity and cost of the processing; in addition, the resulting product shape in the form of a thin sheet significantly limits the real industrial HEAs/MEAs application.

In the last decades, additive manufacturing (AM), also known as three-dimensional (3D) printing, emerged as a modern approach that allows printing metal parts with complex geometry for use in various industries. AM techniques, based on laser-directed energy deposition (L-DED) [25–27] or laser powder bed fusion (LPBF) [28–31], are the most used methods for producing metal parts with enhanced mechanical properties. Although significant progress has been made in the fabrication of M/HEAs using different AM methods [32–34], the strengthening mechanisms that determine the increased strength compared to traditionally produced alloys, are still debated. For example, structures consisting of a large number of dislocation networks or pile-ups, formed by powder bed processes, based on selective laser melting (SLM), provided high dislocation strengthening of M/HEAs [35–37]. Yet, in [38], the strength increment of laser direct energy-deposited CoCrFeNiMn compared with the as-cast alloy was attributed to a finer grain size.

To shed more light on the microstructure–mechanical properties relationships in the AM-processed M/HEAs, in this work, the mechanical behavior of the CoCrFeNi MEA produced by L-DED was investigated during deformation in a temperature range of 77–1073 K. Microstructural evolution and deformation/strengthening mechanisms of the alloy were examined and discussed.

2. Materials and Methods

The Co-Cr-Fe-Ni alloy powder (in equimolar ratio) with a fraction of 50 μm was obtained by the inert gas atomization technology. The CoCrFeNi medium-entropy alloy was deposited using a technological complex with an LS-3 Yb fiber laser (IPG Photonics, Oxford, MA, USA) and industrial robot LRM-200iD_7L (Fanuc, Oshino-mura, Japan) on

an austenitic stainless steel substrate. The sample was produced in a protective argon gas environment. The process was carried out at a power of 1200 W, scanning speed of 20 mm/s, and laser spot size of 2 mm. The hatch spacing and height offset were 1.33 mm and 0.6 mm, respectively. A schematic representation of the deposition strategy is shown in Figure 1a. The as-deposited alloy measured ~50 × 8 × 50 mm^3 (Figure 1b) and had a relative density higher than 99.8%. After L-DED, the CoCrFeNi alloy was subjected to annealing under ambient atmosphere at 1200 °C for 24 h, followed by air-cooling.

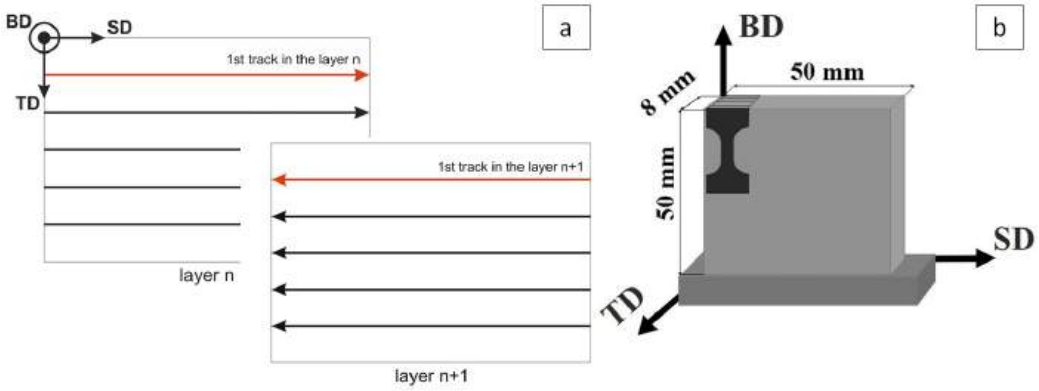

Figure 1. Schematic for the deposition strategy (**a**) and sample fabricated by L-DED (**b**). Here, BD—building direction, SD—scanning direction, and TD—transverse direction.

Tensile tests at temperature range of 77–1073 K were carried out using samples with a gauge dimension of 12 × 5 × 2 mm^3 at an initial strain rate of 1 × 10^{-3} s^{-1} by using the Instron universal testing machine 5882 (Instron, Canton, OH, USA) equipped with a three-zone split furnace. At least 3 specimens were tested for each condition. Microhardness was evaluated using a Future-Tech FM-310 micro-Vickers hardness tester (Future-Tech Corp., Kawasaki, Japan) with a 300 g load. At least 20 measurements per data point were made.

The as-deposited and homogenized microstructures of the CoCrFeNi alloy were investigated in the initial condition and after tensile fracture. Phase identification was performed by X-ray diffraction (XRD) analysis using Bruker D2 Phaser diffractometer (Bruker AXS Gmbh, Karlsruhe, Germany) with Cu-Kα radiation. The structural investigations were carried out in the center of longitudinal (SD-BD) plane using scanning and transmission electron microscope (SEM) and (TEM). SEM-microstructure was studied by Tescan Mira3 LMH (Tescan, Brno, Czech Republic) equipped with an electron backscatter diffraction (EBSD) detector with the Aztec Live Advanced Ultim Max 65 energy dispersive microanalysis system. The 1 × 1 mm EBSD images were collected with a step size of 1 μm. The border between low-angle boundaries (LABs) and high-angle boundaries (HABs) was assumed to be 15°. The special $\Sigma 3^n$ CSL grain boundaries were defined using Brandon's criterion (15° $\Sigma^{-0.5}$). The mean grain size was evaluated as an equivalent diameter of areas bounded by high-angle boundaries with misorientations of $\theta \geq 15°$. The twin density was defined as the ratio of the length of twin boundaries to the scan area.

The TEM studies were performed using a JEOL JEM-2100 microscope (JEOL Ltd., Tokyo, Japan) equipped with an energy dispersive spectrometry (EDS) detector. Specimens for TEM were ground to about 0.1 mm in thickness. Then, the discs with a 3 mm diameter were cut and electropolished to perforation with a Tenupol-5 twinjet polishing unit using a 90% CH_3COOH and 10% $HClO_4$ solution at 25 V at room temperature. The dislocation density was evaluated by counting the number of intersections of dislocations with the foil surfaces using at least five TEM images.

3. Results

The microstructure of the CoCrFeNi medium-entropy alloy after L-DED and L-DED with subsequent annealing at 1200 °C for 24 h is shown in Figure 2. The chemical composition of the alloy, determined by energy dispersive spectrometry (EDS) analysis, corresponded to $Co_{26}Cr_{27}Fe_{21}Ni_{26}$ (in at.%). The as-deposited alloy (Figure 2a) has a single-phase face-centered cubic (fcc) solid solution structure, as confirmed by XRD analysis (Figure 2(a1)). The formation of columnar grains along the BD with an average transverse grain size of about 70 μm due to epitaxial grain growth during L-DED occurred. The inverse pole figure orientation map (IPF) (Figure 2(a2)) indicates a preferred grain orientation close to <100>, which is typical for fast directional grain growth in fcc materials during solidification [39]. The large peak corresponding to the low-angle ($2° \leq \theta < 15°$) sub-boundaries can be recognized in grain boundary misorientation distribution (Figure 2(a3)). Formation of LABs during AM may be caused by high thermal stress resulting in a rapid solidification rate [40], which promotes a high dislocation density (8.1×10^{13} m^{-2}) in the alloy (Figure 2(a4)).

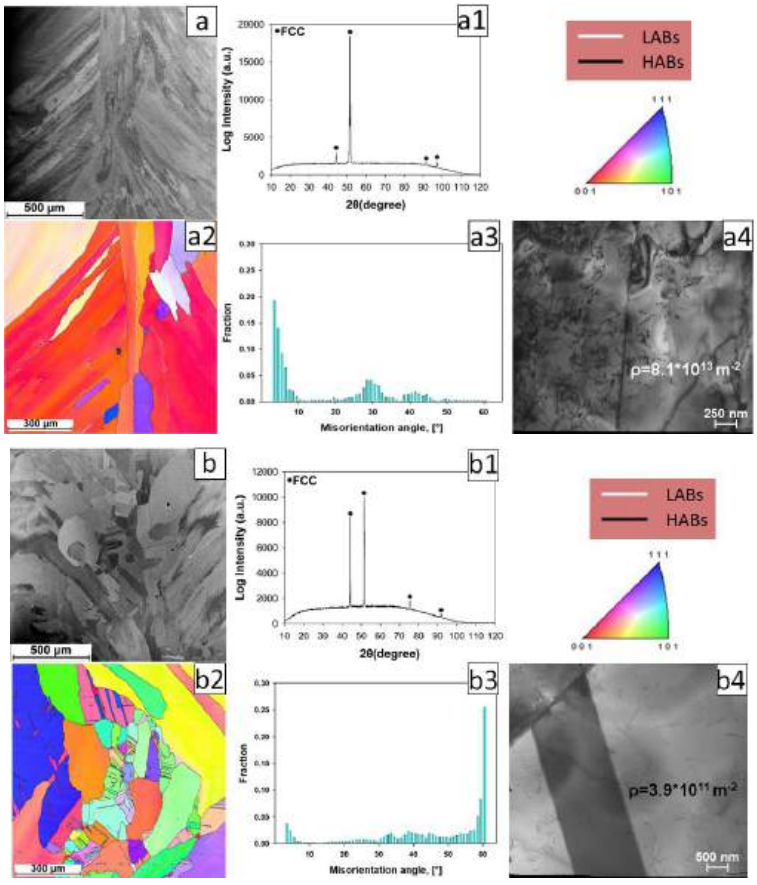

Figure 2. Structure of the (**a**) as-deposited and (**b**) as-deposited and annealed at 1200 °C CoCrFeNi alloy: (**a**,**b**) SEM BSE-microstructure; (**a1**,**b1**) XRD analysis; (**a2**,**b2**) inverse pole figure orientation map; (**a3**,**b3**) grain boundaries misorientation distributions; and (**a4**,**b4**) TEM-microstructure. The black and white lines indicate high-angle boundaries ($\theta \geq 15°$) and low-angle sub-boundaries ($2° \leq \theta < 15°$), respectively.

Annealing of the as-deposited alloy at 1200 °C for 24 h leads to the development of primary recrystallization (Figure 2b) of the single fcc phase structure (Figure 2(b1)). Spheroidization and coarsening of grains to an average size of 180 μm was observed. The structure has a nearly equiaxed morphology, although grains elongated along the BD are also identified. The development of the primary recrystallization is accompanied by a

formation of numerous annealing twins with special Σ3 CSL (coincident site lattice) grain boundaries (Figure 2(b2)), corresponding to a misorientation peak close to 60° (Figure 2(b3)). TEM studies confirmed the formation of annealing twins and a decrease in the dislocation density (Figure 2(b4)). The dislocation density decreased from 8.1 × 10^{13} m^{-2} in the as-deposited state to 3.9 × 10^{11} m^{-2} after annealing.

Figure 3 shows engineering stress–strain curves at various testing temperatures and the mechanical properties, namely the yield strength (YS), ultimate tensile strength (UTS), and total elongation to fracture (TE), for the as-deposited and annealed medium-entropy CoCrFeNi alloy. The mechanical behavior of the alloy shows a general tendency to decrease both the strength and ductility with increasing testing temperature. The as-deposited alloy (Figure 3a,c) demonstrates maximum values of yield and ultimate tensile strengths measured at 565 MPa and 963 MPa during cryogenic (77 K) deformation. The pronounced strain hardening stage results in a high total elongation of 61% and failure without necking. A sharp drop in YS/UTS to 368 MPa and 610 MPa, respectively, was observed as the testing temperature increased to room (293 K), while the total elongations to fracture remained the same value. Deformation at higher temperatures in the range of 473–1073 K resulted in a gradual decrease in flow stress. The uniform elongation of the alloy is significantly reduced during tension at 873 K to 35%. At 1073 K flow stress rapidly increased to a maximum of 213 MPa at strain of 4%, followed by necking and failure at a total elongation of 23%.

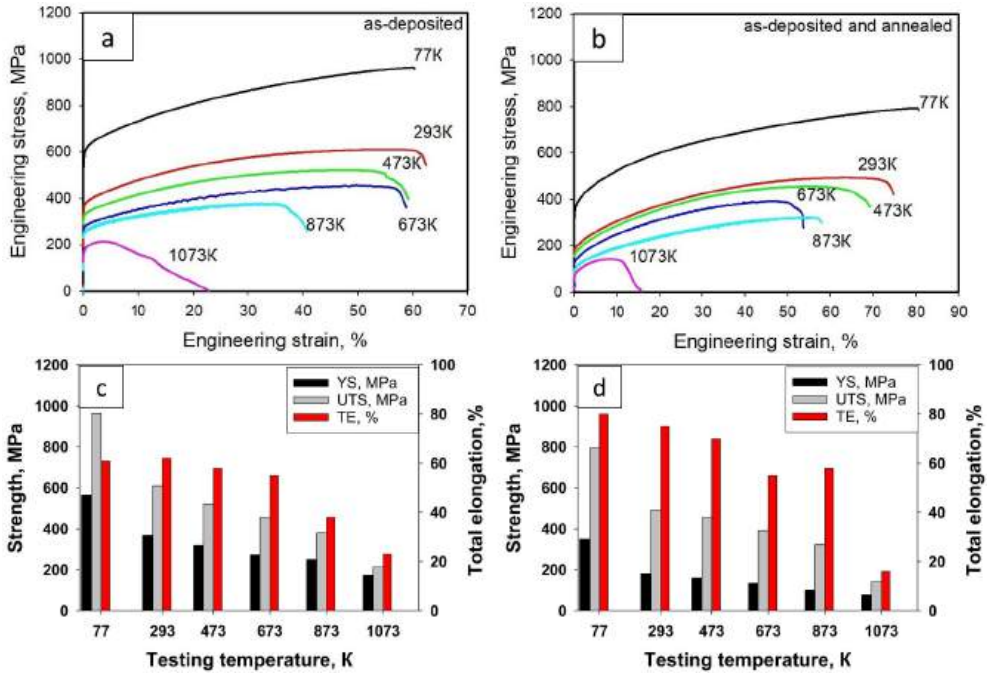

Figure 3. Tensile engineering stress-strain curves (**a**,**b**) and mechanical properties (**c**,**d**) of as-deposited (**a**,**c**) and as-deposited and annealed at 1200 °C (**b**,**d**) CoCrFeNi alloy at different testing temperatures.

The alloy subjected to subsequent annealing exhibits similar mechanical behavior at the same temperatures (Figure 3b). However, compared to the as-deposited alloy, homogenization annealing resulted in softening and increment of ductility during all testing temperatures (Figure 3b). For instance, the values of the yield and ultimate strengths of annealed alloy decreased by ~2 and ~1.2 times, respectively.

The EBSD IPF maps of the deformed microstructure of the as-deposited CoCrFeNi alloy are represented in Figure 4. At cryogenic and room temperatures (Figure 4a,b), the dislocation slip develops along with the intensive deformation twinning (twin boundaries are marked in red in Figure 4(a1,b1)). The fraction of twin boundaries correspond to 11 and 13%, respectively (Figure 4(a3,b3)). Kernel average misorientation (KAM) maps showed a

local grain misorientation, formed by geometrically necessary (GNDs) dislocations. The KAM map of the alloy tested at cryogenic temperature (Figure 4(a2)) demonstrates an uneven distribution of dislocations. Deformed grains, which correspond to higher KAM values, are observed near the fracture surface along with practically undeformed (blue-colored) areas. Increasing the deformation temperature to 293 K leads to a more uniform distribution of the deformed substructure (Figure 4(b2)). After tension at 673 K (Figure 4c), no twin formation is observed, and deformation occurs through only dislocation slip, which is accompanied by an increase in the fraction of LABs. A strong decrease in both average KAM value and LAB fraction after 1073 K (Figure 4d) is probably due to the development of dynamic recovery or dynamic recrystallization of the CoCrFeNi alloy at this temperature.

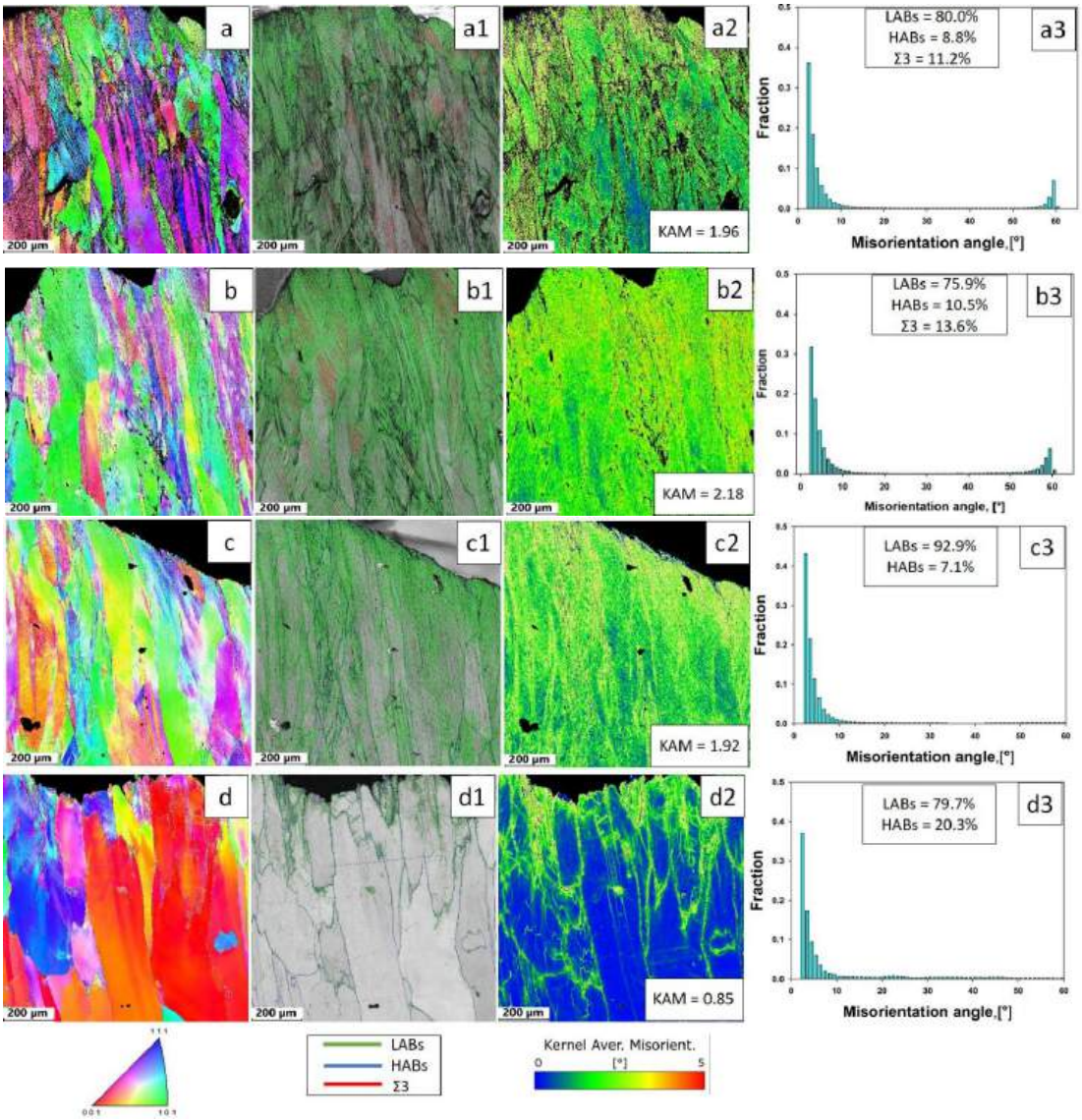

Figure 4. EBSD IPF maps of tensile microstructure of the as-deposited CoCrFeNi alloy tested at (**a**) 77 K; (**b**) 293 K; (**c**) 673 K; and (**d**) 1073 K. (**a1**–**d1**) Quality maps with marked grain boundaries; (**a2**–**d2**) kernel average misorientations maps; and (**a3**–**d3**) grain boundary misorientation distributions. The blue, green, and red lines indicate high-angle boundaries ($\theta \geq 15°$), low-angle sub-boundaries ($2° \leq \theta < 15°$), and special Σ3 CSL grain boundaries, respectively.

The deformed structures after annealing at 1200 °C are shown in Figure 5. Despite the spheroidization of the initial structure during annealing, after deformation, grains are elongated along the tensile direction, although a larger width of grains should be noted. The

recrystallized alloy is intensively twinned at 77 K (Figure 5(a1,a2)), and the fraction of special Σ3 CSL twin boundaries reaches 18%. Despite the apparent decrease in the fraction of twin boundaries compared to the initial state (Figure 2(b2)), the increase in the twin density from 0.024 μm^{-1} (after annealing) to 0.062 μm^{-1} in this case is ensured by the formation of new deformation twins. However, the structure contains areas with small non-twinned grains with a low KAM value, that are not subject to twinning. The absence of twinning in small grains is associated with a significant increase in the critical twinning stress with decreasing grain size [41]. During tension at 293 K (Figure 5b), deformation occurs predominantly through dislocation slip, although the average value of the KAM remains at the same level. Similar to the as-deposited alloy, in the recrystallized one, only dislocation slip is observed after deformation at 673 K (Figure 5c). The structure of the alloy after tension at 1073 K (Figure 5d) is qualitatively similar to the original recrystallized one. The structure is represented by equiaxed grains, which contain several annealing twins. Their density is estimated to be 0.015 μm^{-1}, which is comparable to that of the undeformed state.

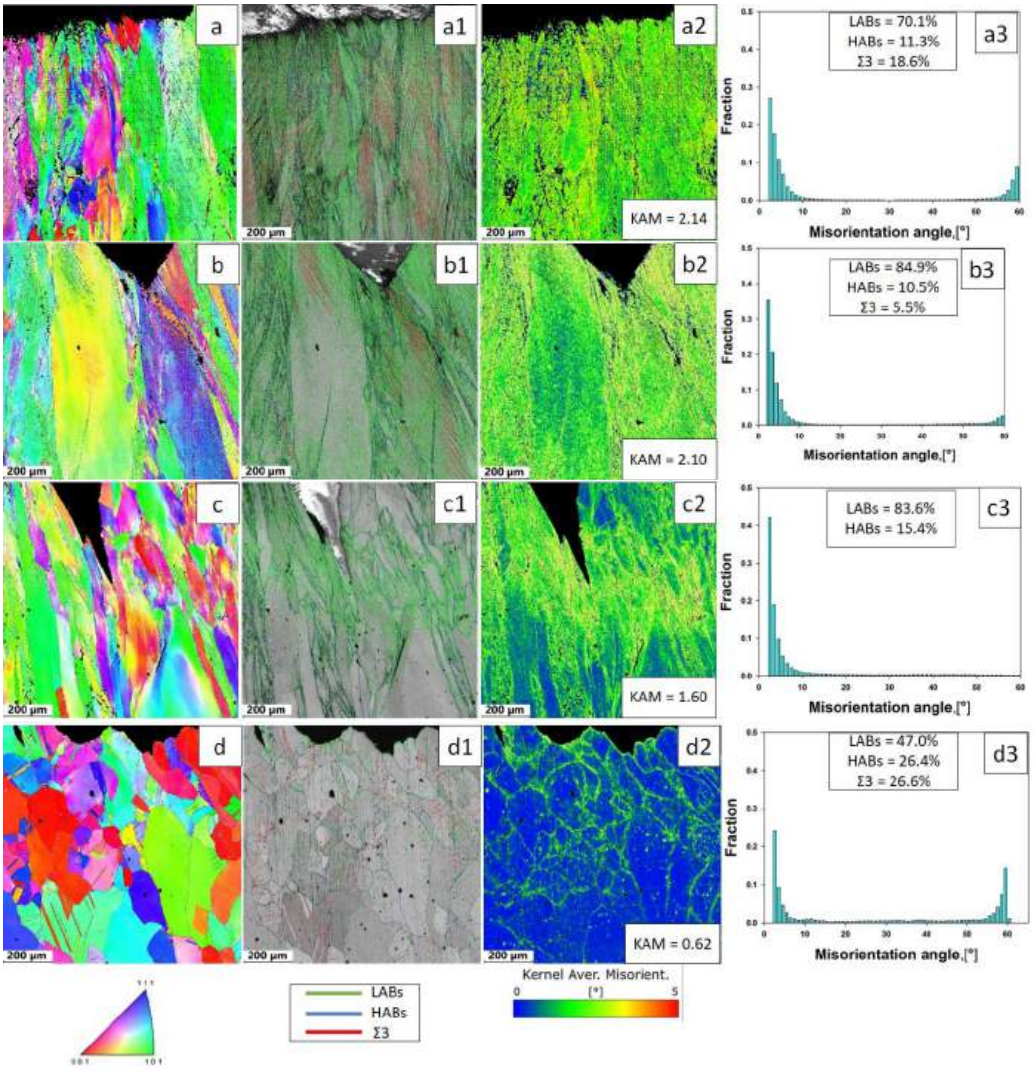

Figure 5. EBSD IPF maps of tensile microstructure of the as-deposited and annealed at 1200 °C CoCrFeNi alloy tested at (**a**) 77 K; (**b**) 293 K; (**c**) 673 K; and (**d**) 1073 K. (**a1**–**d1**) Quality maps with marked grain boundaries; (**a2**–**d2**) kernel average misorientations maps; and (**a3**–**d3**) grain boundary misorientation distributions. The blue, green, and red lines indicate high-angle boundaries ($\theta \geq 15°$), low-angle sub-boundaries ($2° \leq \theta < 15°$), and special Σ3 CSL grain boundaries, respectively.

The microhardness of the alloy near the neck after the tensile test at different temperatures is shown in Figure 6. The microhardness of the as-deposited and annealed alloy in the initial state was 190 and 150 Hv. The cryogenic temperature of deformation leads to a nearly twofold increment of microhardness. A further increase in deformation temperature is expectedly accompanied by a continuous decrease in microhardness due to the softening of alloy, associated with a reduction in the dislocation density and a change in the deformation mechanisms.

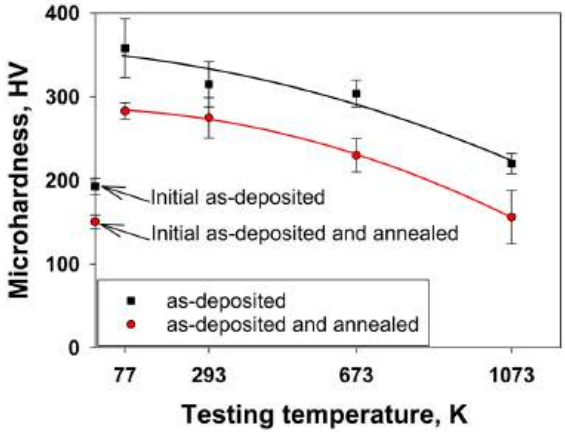

Figure 6. Microhardness of the CoCrFeNi alloy in the initial state and after tensile test at different temperatures.

4. Discussion

In the present work, the mechanical behavior in the temperature range of 77–1073 K of the CoCrFeNi medium-entropy alloy produced by laser-directed energy deposition was investigated. The microstructure of the as-printed alloy was rather typical of the metallic alloys after AM with coarse, elongated grains/subgrains and a high dislocation density. Formation of the columnar structure was ensured by epitaxial grain growth along the BD due to a strong thermal gradient, which is quite typical of the AM processes, based on laser-directed energy deposition [42–44]. Annealing has resulted in the development of primary recrystallization, presumably due to a high aspect ratio of columnar grains and high defect density, which caused the spheroidization of elongated grains and the annihilation of the original dislocation structure.

It is interesting to compare the mechanical properties of the program alloy with those of similar alloys processed by conventional methods [5,15,45,46]. Surprisingly, the YS of the as-printed CoCrFeNi (Figure 7a) is almost identical to that of the Cantor alloy (Figure 7b), produced by arc melting followed by thermomechanical processing (cold rolling with subsequent annealing) [8] despite a significant difference in the grain size between those two alloys: Namely, the as-printed alloy had the coarse grains (70 μm), while the Cantor alloy had a fine-grained structure with an average grain size of 4.4 μm. Meanwhile, the annealed CoCrFeNi alloy with a grain size of 180 μm had comparable properties to the CoCrFeMnNi with a grain size of 155 μm.

To rationalize the effect of the microstructure and testing temperature on the YS of the program alloy, we have further performed a quantitative analysis of strengthening mechanisms. The yield strength of the single-phase CoCrFeNi alloy can be expressed as a sum of dislocation strengthening and grain boundary strengthening:

$$\sigma_{0.2} = \sigma_0 + \Delta\sigma_{H-P} + \Delta\sigma_\rho \quad (1)$$

where σ_0 is the friction stress, $\Delta\sigma_{H-P}$ is the grain boundary strengthening, and $\Delta\sigma_\rho$ is the dislocation strengthening.

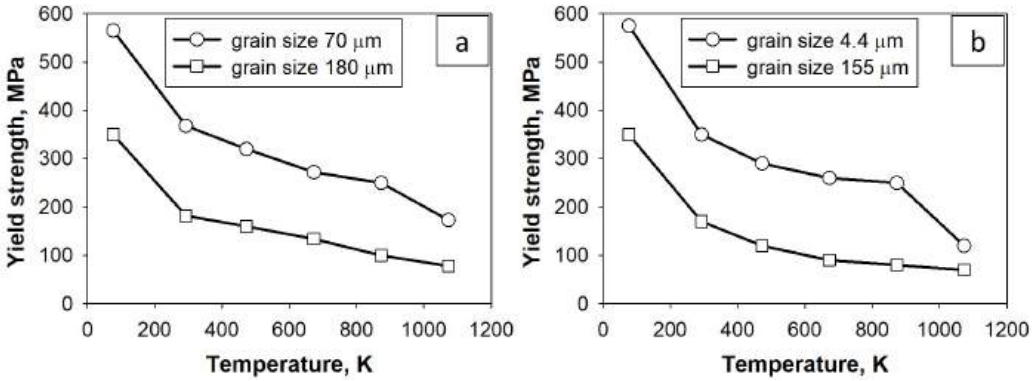

Figure 7. Temperature dependence of the yield stress of the (**a**) as-deposited CoCrFeNi alloy and (**b**) CoCrFeMnNi alloy, processed by conventional methods (adapted from Ref. [8]).

The grain boundary (or grain size) strengthening can be calculated using the second term of the well-known Hall–Petch relationship [47]:

$$\Delta\sigma_{H-P} = k_y\, D^{-1/2} \quad (2)$$

where k_y is a grain boundary strengthening factor, and D is the grain size. The values of 70 μm and 180 μm were used for calculations for the as-deposited and annealed conditions, respectively, in accordance with the results of the microstructural examinations (Figure 2).

The dislocation strengthening can be estimated using the Taylor-type equation [48]:

$$\Delta\sigma_\rho = M\alpha G b\sqrt{\rho} \quad (3)$$

where $M = 3$ is the Taylor factor, $\alpha = 0.3$ is a constant, $b = 2.58 \times 10^{-10}$ m is the Burgers vector [7], G is the shear modulus, and $\rho = 8.1 \times 10^{13}$ m^{-2} and 3.9×10^{11} m^{-2}—dislocation densities in the as-deposited and annealed conditions, respectively.

Using the values of friction stress σ_0 and the coefficient k_y for various temperatures, experimentally determined in [8], and the temperature dependence of the shear modulus described in [49] as $G = 89.4 - 13.0/(e^{373/T} - 1)$, contributions of strengthening mechanisms to yield strengths were calculated. The comparison between the experimental yield strengths (Figure 3c,d) and those calculated by Equation (1) demonstrates a good agreement for the CoCrFeNi alloy in both the as-deposited (Figure 8a) and annealed state (Figure 8b).

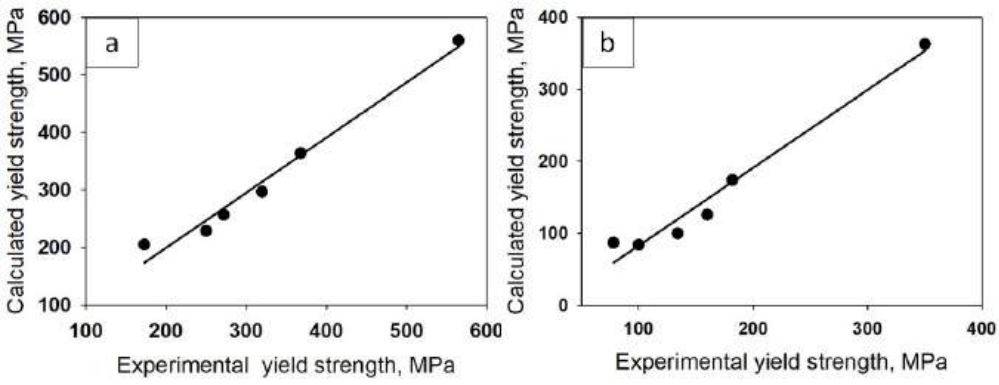

Figure 8. *Cont.*

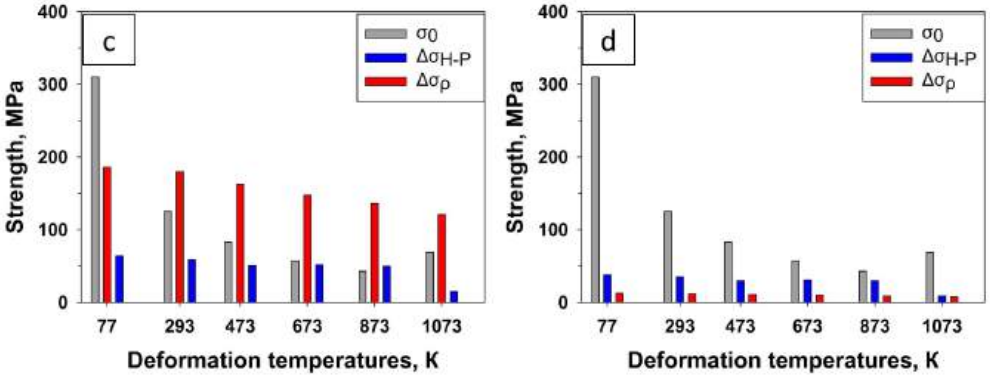

Figure 8. The relationship between experimental and calculated yield strengths (**a**,**b**) and calculated contributions of the grain boundary strengthening and dislocation strengthening (**c**,**d**) of the (**a**,**c**) as-deposited and (**b**,**d**) as-deposited and annealed at 1200 °C CoCrFeNi alloy; friction stress σ_0 values were adapted from Ref. [8].

The calculations have shown that the highest strength increment in the as-deposited alloy (Figure 8c) was provided by dislocation strengthening, which is approximately 3 times higher than the Hall–Petch one. Specifically, in the temperature testing range of 293–1073 K, the dislocation contribution reaches 50–60% of the total strength. At cryogenic temperature (77 K), the lattice friction nonlinearly increases; therefore, σ_0 becomes dominant among all strengthening mechanisms in both states. In addition, homogenization leads to a significant reduction in the initial density of dislocation and grain growth, which results in the change of contribution of the main strengthening mechanism (Figure 8d). Thus, the high dislocation density (~10^{13} m^{-2}), formed due to nonequilibrium conditions during laser-directed energy deposition, provides a significant strength increment compared to traditional processing methods.

To determine the main deformation mechanism (dislocation slip or twinning) at room and cryogenic temperatures, the dislocation density initiated by tensile deformation was assessed. Strain gradient theory indicates that the density of GNDs can be calculated based on the following equation [50]:

$$\rho = {}^{2\theta}/_{bl} \quad (4)$$

where θ is the average Kernel misorientation angle, b is the Burgers vector, and l is the OIM step size.

Densities of geometrically necessary dislocations were calculated as 2.73 × 10^{14} m^{-2} and 3.04 × 10^{14} m^{-2} for the as-deposited alloy deformed at 77 K and 293 K, respectively. Using Equation (3), the strength, introduced by dislocations during deformation at cryogenic and room temperatures, is estimated to be 317 MPa and 334 MPa, which reaches ~33% and ~55% of the ultimate tensile strengths, respectively. These findings confirm the high contribution of twinning at cryogenic deformation, which decreases with increasing temperature. The deformation mechanisms observed in the alloy processed by AM, i.e., deformation twinning at 77 K, dominant dislocation slip at 293–673 K, and initiation of dynamic recovery/recrystallization at 1073 K, also agree reasonably with that reported for conventionally processed Cantor-type alloys [8,51]. A rather surprising observation is the activation of deformation twinning at 293 K in the as-printed alloy, as evidenced by the corresponding grain boundary misorientation distribution (Figure 4(b3)). Note that similar behavior was observed in [32], where twinning is observed from room temperature up to 600 °C during compression testing. In the case of the program CoCrFeNi alloy, the activation of mechanical twinning can be attributed to the below-discussed high flow

stresses, leading to high critical shear resolved stresses necessary to trigger twinning as it was suggested in [52].

5. Conclusions

In this work, the temperature dependence of the mechanical properties of the CoCrFeNi medium-entropy alloy produced by laser-directed energy deposition and further annealing was investigated, and the following conclusions were drawn:

1. The microstructure of CoCrFeNi MEA, fabricated by L-DED, is represented by columnar grains with a transverse size of 70 μm and a high dislocation density of 8.1×10^{13} m^{-2}. Annealing at 1200 °C results in the development of recrystallization, structure coarsening, and a decrease in density of dislocations.
2. The as-deposited CoCrFeNi MEA demonstrates attractive mechanical properties, namely a yield strength of YS = 370/565 and an ultimate tensile strength of 610/965 MPa at 293/77 K, along with a total elongation of 60%. Annealing at 1200 °C leads to significant softening and increased ductility of the CoCrFeNi alloy.
3. Deformation twinning was the main deformation mechanism during testing at 77 K, dominant dislocation slip was observed at 293–673 K, and initiation of dynamic recovery/recrystallization occurred at 1073 K in both the as-deposited and annealed CoCrFeNi alloy.
4. The contribution of dislocation strengthening caused by the high dislocation density after L-DED plays the dominant role in the increased yield strength of the as-deposited CoCrFeNi alloy compared with the similar alloy processed by conventional techniques.

To sum up, this study has shown that coarse-grained fcc M/HEAs after laser-directed energy deposition can have tensile properties comparable to the similar alloys in the fine-grained condition after conventional thermomechanical processing due to significant dislocation density formed during the AM process. This finding can open up new routes for the additive manufacturing of parts of complex geometries from advanced alloys.

Author Contributions: Conceptualization, M.K. and S.Z.; methodology, E.K. (Elizaveta Kochura) and A.S.; validation, O.K.-K. and A.S.; formal analysis, I.K., E.K. (Elizaveta Kochura) and A.S.; investigation, I.K., I.A. and E.K. (Ekaterina Kovalenko); data curation, M.K., E.K. (Ekaterina Kovalenko) and N.S.; writing—original draft preparation, M.K.; writing—review and editing, S.Z. and N.S.; visualization, I.K., I.A. and E.K. (Elizaveta Kochura); supervision, N.S.; project administration, O.K.-K. All authors have read and agreed to the published version of the manuscript.

Funding: This research was funded by the Russian Science Foundation (Grant No. 20-79-10093). The TEM work was partially funded by the Ministry of Science and Higher Education of the Russian Federation within the framework of the «World-class Science Center» Program: Advanced Digital Technologies (Grant Agreement No. 075-15-2022-312, 20 April 2022).

Data Availability Statement: The original contributions presented in this study are included in the article. Further inquiries can be directed to the corresponding author.

Conflicts of Interest: The authors declare no conflicts of interest.

References

1. Yeh, J.-W.; Chen, S.-K.; Lin, S.-J.; Gan, J.-Y.; Chin, T.-S.; Shun, T.-T.; Tsau, C.-H.; Chang, S.-Y. Nanostructured High-Entropy Alloys with Multiple Principal Elements: Novel Alloy Design Concepts and Outcomes. *Adv. Eng. Mater* **2004**, *6*, 299–303. [CrossRef]
2. Cantor, B.; Chang, I.T.H.; Knight, P.; Vincent, A.J.B. Microstructural development in equiatomic multicomponent alloys. *Mater. Sci. Eng. A* **2004**, *375*, 213–218. [CrossRef]

3. Otto, F.; Yang, Y.; Bei, H.; George, E.P. Relative Effects of Enthalpy and Entropy on the Phase Stability of Equiatomic High-Entropy Alloys. *Acta Mater.* **2013**, *61*, 2628–2638. [CrossRef]
4. Miracle, D.B.; Senkov, O.N. A critical review of high entropy alloys and related concepts. *Acta Mater.* **2017**, *122*, 448–511. [CrossRef]
5. Salishchev, G.A.; Tikhonovsky, M.A.; Shaysultanov, D.G.; Stepanov, N.D.; Kuznetsov, A.V.; Kolodiy, I.V.; Tortika, A.S.; Senkov, O.N. Effect of Mn and V on Structure and Mechanical Properties of High-Entropy Alloys Based on CoCrFeNi System. *J. Alloys Compd.* **2014**, *591*, 11–21. [CrossRef]
6. Otto, F.; Dlouhý, A.; Pradeep, K.G.; Kuběnová, M.; Raabe, D.; Eggeler, G.; George, E.P. Decomposition of the Single-Phase High-Entropy Alloy CrMnFeCoNi after Prolonged Anneals at Intermediate Temperatures. *Acta Mater.* **2016**, *112*, 40–52. [CrossRef]
7. Pickering, E.J.; Muñoz-Moreno, R.; Stone, H.J.; Jones, N.G. Precipitation in the Equiatomic High-Entropy Alloy CrMnFeCoNi. *Scr. Mater.* **2016**, *113*, 106–109. [CrossRef]
8. Otto, F.; Dlouhý, A.; Somsen, C.; Bei, H.; Eggeler, G.; George, E.P. The influences of temperature and microstructure on the tensile properties of a CoCrFeMnNi high-entropy alloy. *Acta Mater.* **2013**, *61*, 5743–5755. [CrossRef]
9. Wu, Z.; Bei, H.; Pharr, G.M.; George, E.P. Temperature Dependence of the Mechanical Properties of Equiatomic Solid Solution Alloys with Face-Centered Cubic Crystal Structures. *Acta Mater.* **2014**, *81*, 428–441. [CrossRef]
10. Klimova, M.V.; Shaysultanov, D.G.; Chernichenko, R.S.; Sanin, V.N.; Stepanov, N.D.; Zherebtsov, S.V.; Belyakov, A.N. Recrystallized Microstructures and Mechanical Properties of a C-Containing CoCrFeNiMn-Type High-Entropy Alloy. *Mater. Sci. Eng. A* **2019**, *740–741*, 201–210. [CrossRef]
11. Li, Z.; Pradeep, K.G.; Deng, Y.; Raabe, D.; Tasan, C.C. Metastable High-Entropy Dual-Phase Alloys Overcome the Strength–Ductility Trade-Off. *Nature* **2016**, *534*, 227–230. [CrossRef] [PubMed]
12. He, Z.F.; Jia, N.; Ma, D.; Yan, H.L.; Li, Z.M.; Raabe, D. Joint contribution of transformation and twinning to the high strength-ductility combination of a FeMnCoCr high entropy alloy at cryogenic temperatures. *Mater. Sci. Eng. A* **2019**, *759*, 437–447. [CrossRef]
13. Zhang, Z.; Sheng, H.; Wang, Z.; Gludovatz, B.; Zhang, Z.; George, E.P.; Yu, Q.; Mao, S.X.; Ritchie, R.O. Dislocation mechanisms and 3D twin architectures generate exceptional strength-ductility-toughness combination in CrCoNi medium-entropy alloy. *Nat. Commun.* **2017**, *8*, 14390. [CrossRef] [PubMed]
14. Laplanche, G.; Kostka, A.; Reinhart, C.; Hunfeld, J.; Eggeler, G.; George, E.P. Reasons for the superior mechanical properties of medium-entropy CrCoNi compared to high-entropy CrMnFeCoNi. *Acta Mater.* **2017**, *128*, 292–303. [CrossRef]
15. Stepanov, N.D.; Tikhonovsky, M.A.; Yurchenko, N.Y.; Zyabkin, D.V.; Klimova, M.V.; Zherebtsov, S.V.; Efimov, A.A.; Salishchev, G.A. Effect of cryo-deformation on structure and properties of CoCrFeNiMn high-entropy alloy. *Intermetallics* **2015**, *59*, 8–17. [CrossRef]
16. Jo, Y.H.; Jung, S.; Choi, W.M.; Sohn, S.S.; Kim, H.S.; Lee, B.J.; Kim, N.J.; Lee, S. Cryogenic strength improvement by utilizing room-temperature deformation twinning in a partially recrystallized VCrMnFeCoNi high-entropy alloy. *Nat. Commun.* **2017**, *8*, 15719. [CrossRef]
17. Joo, S.H.; Kato, H.; Jang, M.J.; Moon, J.; Tsai, C.W.; Yeh, J.W.; Kim, H.S. Tensile deformation behavior and deformation twinning of an equimolar CoCrFeMnNi high-entropy alloy. *Mater. Sci. Eng. A* **2017**, *689*, 122–133. [CrossRef]
18. Zaddach, A.J.; Niu, C.; Koch, C.C.; Irving, D.L. Mechanical Properties and Stacking Fault Energies of NiFeCrCoMn High-Entropy Alloy. *JOM* **2013**, *65*, 1780–1789. [CrossRef]
19. Huang, S.; Li, W.; Lu, S.; Tian, F.; Shen, J.; Holmström, E.; Vitos, L. Temperature dependent stacking fault energy of FeCrCoNiMn high entropy alloy. *Scr. Mater.* **2015**, *108*, 44–47. [CrossRef]
20. Gludovatz, B.; Hohenwarter, A.; Catoor, D.; Chang, E.H.; George, E.P.; Ritchie, R.O. A fracture-resistant high-entropy alloy for cryogenic applications. *Science* **2014**, *345*, 1153–1158. [CrossRef]
21. Zhang, Z.; Mao, M.M.; Wang, J.; Gludovatz, B.; Zhang, Z.; Mao, S.X.; George, E.P.; Yu, Q.; Ritchie, R.O. Nanoscale origins of the damage tolerance of the high-entropy alloy CrMnFeCoNi. *Nat. Commun.* **2015**, *6*, 10143. [CrossRef] [PubMed]
22. Stepanov, N.D.; Shaysultanov, D.G.; Chernichenko, R.S.; Ikornikov, D.M.; Sanin, V.N.; Zherebtsov, S.V. Mechanical properties of a new high entropy alloy with a duplex ultra-fine grained structure. *Mater. Sci. Eng. A* **2018**, *728*, 54–62. [CrossRef]
23. Klimova, M.V.; Shaysultanov, D.G.; Semenyuk, A.O.; Zherebtsov, S.V.; Stepanov, N.D. Effect of carbon on recrystallised microstructures and properties of CoCrFeMnNi-type high-entropy alloys. *J. Alloys Compd.* **2021**, *851*, 156839. [CrossRef]
24. Sun, S.J.; Tian, Y.Z.; Lin, H.R.; Dong, X.G.; Wang, Y.H.; Zhang, Z.J.; Zhang, Z.F. Enhanced strength and ductility of bulk CoCrFeMnNi high entropy alloy having fully recrystallized ultrafine-grained structure. *Mater. Des.* **2017**, *133*, 122–127. [CrossRef]
25. Xiang, S.; Luan, H.; Wu, J.; Yao, K.F.; Li, J.; Liu, X.; Tian, Y.; Mao, W.; Bai, H.; Le, G.; et al. Microstructures and mechanical properties of CrMnFeCoNi high entropy alloys fabricated using laser metal deposition technique. *J. Alloys Compd.* **2019**, *773*, 387–392. [CrossRef]

26. Weng, F.; Chew, Y.; Zhu, Z.; Yao, X.; Wang, L.; Ng, F.L.; Liu, S.; Bi, G. Excellent combination of strength and ductility of CoCrNi medium entropy alloy fabricated by laser aided additive manufacturing. *Addit. Manuf.* **2020**, *34*, 101202. [CrossRef]
27. Xiang, S.; Li, J.; Luan, H.; Amar, A.; Lu, S.; Li, K.; Zhang, L.; Liu, X.; Le, G.; Wang, X.; et al. Effects of process parameters on microstructures and tensile properties of laser melting deposited CrMnFeCoNi high entropy alloys. *Mater. Sci. Eng. A* **2019**, *743*, 412–417. [CrossRef]
28. Wang, Y.M.; Voisin, T.; McKeown, J.T.; Ye, J.; Calta, N.P.; Li, Z.; Zeng, Z.; Zhang, Y.; Chen, W.; Roehling, T.T.; et al. Additively manufactured hierarchical stainless steels with high strength and ductility. *Nat. Mater.* **2018**, *17*, 63–71. [CrossRef]
29. Lin, W.C.; Chang, Y.J.; Hsu, T.H.; Gorsse, S.; Sun, F.; Furuhara, T.; Yeh, A.C. Microstructure and Tensile Property of a Precipitation Strengthened High Entropy Alloy Processed by Selective Laser Melting and Post Heat Treatment. *Addit. Manuf.* **2020**, *36*, 101601. [CrossRef]
30. Zhu, Z.G.; Nguyen, Q.B.; Ng, F.L.; An, X.H.; Liao, X.Z.; Liaw, P.K.; Nai, S.M.L.; Wei, J. Hierarchical microstructure and strengthening mechanisms of a CoCrFeNiMn high entropy alloy additively manufactured by selective laser melting. *Scr. Mater.* **2018**, *154*, 20–24. [CrossRef]
31. Wang, J.; Zou, J.; Yang, H.; Zhang, L.; Liu, Z.; Dong, X.; Ji, S. Exceptional Strength-Ductility Synergy of Additively Manufactured CoCrNi Medium-Entropy Alloy Achieved by Lattice Defects in Heterogeneous Microstructures. *J. Mater. Sci. Technol.* **2022**, *127*, 61–70. [CrossRef]
32. Kim, Y.-K.; Yang, S.; Lee, K.-A. Superior Temperature-Dependent Mechanical Properties and Deformation Behavior of Equiatomic CoCrFeMnNi High-Entropy Alloy Additively Manufactured by Selective Laser Melting. *Sci. Rep.* **2020**, *10*, 8045. [CrossRef]
33. Brif, Y.; Thomas, M.; Todd, I. The Use of High-Entropy Alloys in Additive Manufacturing. *Scr. Mater.* **2015**, *99*, 93–96. [CrossRef]
34. Lin, D.; Xu, L.; Jing, H.; Han, Y.; Zhao, L.; Minami, F. Effects of Annealing on the Structure and Mechanical Properties of FeCoCrNi High-Entropy Alloy Fabricated via Selective Laser Melting. *Addit. Manuf.* **2020**, *32*, 101058. [CrossRef]
35. Lin, D.; Xu, L.; Han, Y.; Zhang, Y.; Jing, H.; Zhao, L.; Minami, F. Structure and Mechanical Properties of a FeCoCrNi High-Entropy Alloy Fabricated via Selective Laser Melting. *Intermetallics* **2020**, *127*, 106963. [CrossRef]
36. Lin, D.; Xi, X.; Li, X.; Hu, J.; Xu, L.; Han, Y.; Zhang, Y.; Zhao, L. High-Temperature Mechanical Properties of FeCoCrNi High-Entropy Alloys Fabricated via Selective Laser Melting. *Mater. Sci. Eng. A* **2022**, *832*, 142354. [CrossRef]
37. Li, R.; Niu, P.; Yuan, T.; Cao, P.; Chen, C.; Zhou, K. Selective Laser Melting of an Equiatomic CoCrFeMnNi High-Entropy Alloy: Processability, Non-Equilibrium Microstructure and Mechanical Property. *J. Alloys Compd.* **2018**, *746*, 125–134. [CrossRef]
38. Chew, Y.; Bi, G.J.; Zhu, Z.G.; Ng, F.L.; Weng, F.; Liu, S.B.; Nai, S.M.L.; Lee, B.Y. Microstructure and Enhanced Strength of Laser Aided Additive Manufactured CoCrFeNiMn High Entropy Alloy. *Mater. Sci. Eng. A* **2019**, *744*, 137–144. [CrossRef]
39. Ma, D.; Stoica, A.D.; Wang, Z.; Beese, A.M. Crystallographic texture in an additively manufactured nickel-base superalloy. *Mater. Sci. Eng. A* **2017**, *684*, 47–53. [CrossRef]
40. Yan, S.; He, X.; Krüger, M.; Li, Y.; Jia, Q. Additive manufacturing of a new non-equiatomic high-entropy alloy with exceptional strength-ductility synergy via in-situ alloying. *Mater. Des.* **2024**, *238*, 112676. [CrossRef]
41. Wagner, C.; Laplanche, G. Effect of Grain Size on Critical Twinning Stress and Work Hardening Behavior in the Equiatomic CrMnFeCoNi High-Entropy Alloy. *Int. J. Plast.* **2023**, *166*, 103651. [CrossRef]
42. Arif, Z.U.; Khalid, M.Y.; Rehman, E. Laser-Aided Additive Manufacturing of High Entropy Alloys: Processes, Properties, and Emerging Applications. *J. Manuf. Process.* **2022**, *78*, 131–171. [CrossRef]
43. Zheng, M.; Li, C.; Zhang, X.; Ye, Z.; Yang, X.; Gu, J. The Influence of Columnar to Equiaxed Transition on Deformation Behavior of FeCoCrNiMn High Entropy Alloy Fabricated by Laser-Based Directed Energy Deposition. *Addit. Manuf.* **2021**, *37*, 101660. [CrossRef]
44. Liu, P.; Wang, Z.; Xiao, Y.; Horstemeyer, M.F.; Cui, X.; Chen, L. Insight into the Mechanisms of Columnar to Equiaxed Grain Transition during Metallic Additive Manufacturing. *Addit. Manuf.* **2019**, *26*, 22–29. [CrossRef]
45. Gali, A.; George, E.P. Tensile properties of high-and medium-entropy alloys. *Intermetallics* **2013**, *39*, 74–78. [CrossRef]
46. Klimova, M.V.; Shaysultanov, D.G.; Zherebtsov, S.V.; Stepanov, N.D. Effect of Second Phase Particles on Mechanical Properties and Grain Growth in a CoCrFeMnNi High Entropy Alloy. *Mater. Sci. Eng. A* **2019**, *748*, 228–235. [CrossRef]
47. Hall, E.O. The Deformation and Ageing of Mild Steel: III Discussion of Results. *Proc. Phys. Soc. B* **1951**, *64*, 747. [CrossRef]
48. Gladman, T. Precipitation hardening in metals. *Mater. Sci. Technol.* **1999**, *15*, 30–36. [CrossRef]
49. Laplanche, G.; Gadaud, P.; Bärsch, C.; Demtröder, K.; Reinhart, C.; Schreuer, J.; George, E.P. Elastic Moduli and Thermal Expansion Coefficients of Medium-Entropy Subsystems of the CrMnFeCoNi High-Entropy Alloy. *J. Alloys Compd.* **2018**, *746*, 244–255. [CrossRef]
50. Calcagnotto, M.; Ponge, D.; Demir, E.; Raabe, D. Orientation Gradients and Geometrically Necessary Dislocations in Ultrafine Grained Dual-Phase Steels Studied by 2D and 3D EBSD. *Mater. Sci. Eng. A* **2010**, *527*, 2738–2746. [CrossRef]

51. Stepanov, N.D.; Shaysultanov, D.G.; Yurchenko, N.Y.; Zherebtsov, S.V.; Ladygin, A.N.; Salishchev, G.A.; Tikhonovsky, M.A. High temperature deformation behavior and dynamic recrystallization in CoCrFeNiMn high entropy alloy. *Mater. Sci. Eng. A* **2015**, *636*, 188–195. [CrossRef]
52. Laplanche, G.; Kostka, A.; Horst, O.M.; Eggeler, G.; George, E.P. Microstructure Evolution and Critical Stress for Twinning in the CrMnFeCoNi High-Entropy Alloy. *Acta Mater.* **2016**, *118*, 152–163. [CrossRef]